Application of a New Numerical Solver to the Simulation of MPD Flows*

K. Sankaran† **E.Y. Choueiri**‡ and **S.C. Jardin**§
Princeton University, Princeton, New Jersey 08544

AIAA-2000-3537¶

July 18, 2000

Abstract

This paper describes the application of a new scheme, that was developed for the solution of the MHD equations, to simulate magnetoplasmadynamic thruster (MPDT) flows. In this scheme, the entire set of flow and field equations are solved in a self-consistent conservation form, using accurate characteristics-splitting techniques which have been proven to be effective in computational fluid dynamics. Further improvements to the physical model, such as the inclusion of real equation of state, anomalous transport and multi-temperature effects, are essential for the realistic simulation magnetoplasmadynamic flows, and are implemented without affecting the underlying scheme. The solver, including the improved physical model, is then used to simulate plasma flow in a real MPDT configuration. The results of the simulation were found to to be in general agreement with experimental observations. They illustrate the need for using a real equation of state, instead of the ideal one, to enhance the realism and stability of the simulation.

1 Introduction

1.1 Motivation

The electrical power deposited into the plasma can be expended into many sinks, but as shown in Fig.(1), only two of which, directed electromagnetic kinetic power and directed electrothermal kinetic power, are useful for propulsion. Understanding and quantifying these disparate processes is essential to improving the efficiency of these devices. Since an empirical approach alone is not generally conducive to obtaining such detailed information on these physical processes, numerical simulations are valuable tools in plasma thruster research. Given the dearth of high power test facilities, simulations can be valuable aides to research by reducing the need for expensive, and sometimes unviable, experimen-

*Research supported by NASA-JPL's Advanced Propulsion Group.

†Graduate Student, MAE Dept. Member AIAA.

‡Chief Scientist at EPPDyL. Assistant Professor, MAE Dept. Senior Member AIAA.

§Principal Research Scientist, Princeton Plasma Physics Lab; Professor, Astrophysical Sciences Dept.

¶Presented at the 36^{th} Joint Propulsion Conference, Huntsville, AL, July 16-19, 2000.

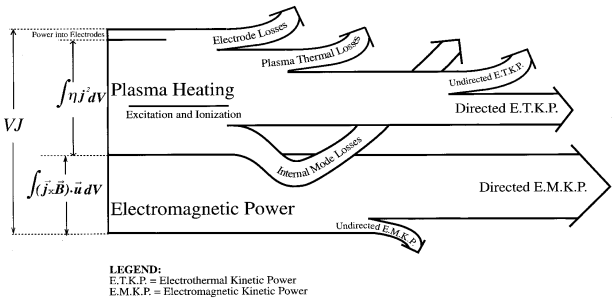

Figure 1: Expenditure of input power in an electromagnetic accelerator (not to scale, from ref.[1]).

tal parametric studies.

The goal of this work is to develop a robust numerical solver for the simulation of plasma flows in MPD thrusters, and apply it to investigate the role of physical processes in these devices.

1.2 Existing Work

There have been several notable efforts to develop numerical models for plasma flows in MPDTs, which will be summarized here.

Kimura $et\ al.$[2], and Fujiwara[3] started developing single-temperature, 2-D models on simple geometries, and have continued to make improvements to their models. Currently, the efforts of Fujiwara $et\ al.$[4] are directed at studying critical phenomena in magnetoplasmadynamic thrusters (MPDT), using multi-temperature models. Caldo and Choueiri[5] have developed a two-temperature model to study the effects of anomalous transport, described in ref.[6], on MPD flows. The effort by LaPointe[7] focused on studying the effect of geometry on performance. Martinez-Sanchez $et\ al.$[8],[9] have developed multi-temperature axisymmetric numerical models to study various aspects of the flow. Turchi[10] $et\ al.$ use MACH2, an unsteady MHD solver developed for high power plasma gun simulation, to model PPTs and MPD thrusters in many geometries. MACH3[11], the next generation of MACH2, is also used to simulate possible 3-D effects in specific situations. The most persistent effort so far has been that of Auweter-Kurtz $et\ al.$[12],[13], who have been developing numerical models for MPD thrusters for almost two decades. Detailed models for many transport processes and multiple levels of ionization have been incorporated into their governing equations, which are solved on unstructured adaptive grids for various geometries.

1.3 Current Approach

Despite these efforts, there remains a need for accurate and robust numerical schemes to simulate propulsive plasma flows. In particular, improvements are required in three aspects:

1. Some of the above mentioned codes exhibit numerical instabilities at high current levels. Since MPD thrusters perform better at higher currents, and many of the important research questions, such as performance limiting phenomena, tend to also occur at higher currents, it is important to be able to simulate at high values of $J^2/\dot{m}$.

   A probable explanation for these numerical instabilities is the failure to solve the magnetic field evolution self-consistently with the flow. The magnetic Reynolds' numbers in typical MPD plasmas indicate that both convective and resistive diffusion of the magnetic field are important, and the corresponding time scales are not very far off.

   Solving Maxwell's equations consistently with compressible gasdynamics equations produces waves physically associated with the problem, such as Alfvèn and magnetosonic waves, as

eigenvalues. Such a formulation is thus suitable for handling MHD waves and shocks.

2. Some of the earlier efforts have experienced problems conserving mass, momentum, and energy. The conservative formulation of the governing equations, used in this work, ensures that these quantities are indeed conserved. From the perspective of numerical solution, it can be shown that conservative formulation is necessary for accurately capturing discontinuities.

3. Though noted earlier[9], none of the existing models (with the exception of recent work of Heiermann[13]) take advantage of the developments in the techniques for numerical solution of Euler and Navier-Stokes equations.

A new solver, developed based on principles mentioned above, was introduced by the authors in ref.[14], and validated in ref.[15]. The focus of this paper is to demonstrate the utility of this solver to investigate plasma flows in MPD thrusters.

1.4 Outline

The underlying scheme is briefly explained using a simplified flow problem in §2. Subsequent improvements to the physical models, that did not require significant changes to the underlying numerical building blocks of the solver, were implemented and are described in §3. The results from the computation of plasma flows in an MPD thruster, using the models described, are presented in §4.1. The effects of some aspects of the model, specifically the equation of state, is investigated in §4.2.

2 MHD Simulations

The solver developed in this work can be illustrated with the simple flow problem of a fully ionized, quasi-neutral plasma in thermal equilibrium under conditions for which the continuum treatment is valid.

2.1 Governing Equations

The governing equations for this problem can be written in the form:

$$\frac{\partial}{\partial t}\begin{bmatrix}\rho\\ \rho\mathbf{u}\\ \mathbf{B}\\ \mathcal{E}\end{bmatrix} + \nabla\cdot\begin{bmatrix}\rho\mathbf{u}\\ \rho\mathbf{u}\mathbf{u}+\bar{\bar{p}}-\bar{\bar{\mathcal{B}}}_M\\ \mathbf{u}\mathbf{B}-\mathbf{B}\mathbf{u}\\ (\mathcal{E}+p)\,\mathbf{u}-\bar{\bar{\mathcal{B}}}_M\cdot\mathbf{u}\end{bmatrix} = \mathbf{S}. \quad (1)$$

The right hand side of the equation, $\mathbf{S}$, contains the dissipative effects that are physical in nature,

$$\mathbf{S} = \nabla\cdot\begin{bmatrix}0\\ \bar{\bar{\tau}}_{vis}\\ \bar{\bar{E}}_{res}\\ \mathbf{q}\end{bmatrix}. \quad (2)$$

In the total continuity relation, any possible diffusion effects are neglected.

The momentum equation contains the electromagnetic body force per unit volume, $\mathbf{j}\times\mathbf{B}$, written as the divergence of the Maxwell stress tensor $\bar{\bar{\mathcal{B}}}_M$, as described in ref.[16]. Here, $\bar{\bar{p}}$ is the isotropic thermodynamic pressure tensor. The viscous stress tensor, $\bar{\bar{\tau}}_{vis}$, can also be included in this formulation, though it is neglected in the results shown in this paper.

In Faraday's law, the convective diffusion of the magnetic field, which is the contribution of the back EMF, is written as a divergence of the antisymmetric tensor $\mathbf{u}\mathbf{B}-\mathbf{B}\mathbf{u}$. The resistive diffusion appears as divergence of the resistive diffusion tensor, $\bar{\bar{E}}_{res}$, as in done ref.[17], which includes the dispersive Hall effect.

The energy equation is written in terms of the energy density (energy per unit volume), $\mathcal{E}$, which includes the internal energy, kinetic energy and the energy in the magnetic field.

Apart from the familiar convective flux of energy, $(\mathcal{E}+p)\,\mathbf{u}$, the other terms are the energy expended in electromagnetic acceleration, $\bar{\bar{\mathcal{B}}}_M \cdot \mathbf{u}$, and the dissipative flux of energy, $\nabla \cdot \mathbf{q}$, due to viscous heating, Ohmic heating, and thermal conduction,

$$\nabla \cdot \mathbf{q} = \nabla \cdot \left[\bar{\bar{\tau}}_{vis} \cdot \mathbf{u} + \frac{\mathbf{B} \times \mathbf{E}'}{\mu_0} + \bar{\bar{\kappa}}_{th} \cdot \nabla T \right] \ ,$$

where $\mathbf{E}'$ is the effective electric field on the plasma.

Under some physical conditions, when the magnetic pressure is several orders of magnitude larger than thermodynamic pressure, the conservation form of the energy equation may not be suitable. In these cases, since the thermodynamic pressure, p, is calculated by subtracting one large number ($B^2/2\mu_o$) from another ($\mathcal{E}$), the associated errors could be large. However, for the conditions that are of interest to plasma propulsion, the magnetic pressure is seldom two orders of magnitude greater than thermodynamic pressure. Thus the conservation form of the energy equation is numerically suitable here.

Thus, the entire set of equations can be written in the conservation form,

$$\frac{\partial \mathbf{U}}{\partial t} + \nabla \cdot \left[\mathcal{F}_{conv} - \mathcal{F}_{diss} \right] \ , \tag{3}$$

where $\mathcal{F}_{conv}$ is the convective flux tensor, and $\mathcal{F}_{diss}$ is the dissipative flux tensor.

2.2 Numerical Solution

The equations described in §2 contain hyperbolic and parabolic PDEs. Much of the discussion in this section will be on the techniques for solving the convective part of the problem. One reason for this is that the goal of this work is to simulate problems in propulsion and therefore computing the flow is the most important part. More importantly, it is this part of the problem that has required improvements. The dissipative part of the problem, which brings in a parabolic nature to the governing equations, is relatively well understood.

2.2.1 Spatial Discretization

There are two important issues in the design of discretization schemes:

- Estimating the numerical flux through cell boundaries, by accounting for waves propagating at different speeds, and possibly in different directions,
- Obtaining non-oscillatory solutions and capturing discontinuities with sufficient accuracy.

The numerical scheme used in this work is derived from research based on the pioneering work of Godunov [18], [19]. The characteristics-splitting technique, which will be described later, was first developed[20], [21] to solve problems in compressible fluid dynamics. It satisfies the Rankine-Hugoniot jump conditions exactly, and has been proven to work reliably for solving the Navier-Stokes equations. Jameson[22] has shown that this scheme can be combined with flux limited anti-diffusion to provide higher order accuracy in smooth regions of the flow, and ensure that there are no unbounded local oscillations.

The essence of this scheme is to split the characteristics based on their direction of propagation. Then, the flux across a cell face, for example whose normal is in the $\hat{z}$ direction, can be split as,

$$\mathbf{Fz}(\mathbf{U}) = \mathbf{Fz}(\mathbf{U})^+ + \mathbf{Fz}(\mathbf{U})^-, \tag{4}$$

where the eigenvalues of $d\mathbf{Fz}^+/d\mathbf{U}$ are all non-negative, and the eigenvalues of $d\mathbf{Fz}^-/d\mathbf{U}$ are all non-positive.

Godunov's theorem[18] assures that no scheme can be better than first order accurate near discontinuities. However, away from the discontinuities,

the spatial accuracy of this scheme can be improved by including flux-limited anti-diffusion, as described in ref.[22]. Details of this implementation, along with test cases for its validation, are documented in ref.[15].

Numerical methods for diffusion type problems are relatively commonplace. Explicit centered spatial differences for the parabolic terms is used in this work, with a sub-stepping method discussed in §2.2.2.

2.2.2 Temporal Discretization

Unlike in fluid mechanics, the equations of MHD allow many different types of waves to exist. Even though physically the flow velocity is the sought quantity of most interest to propulsion, numerically the velocity of the fastest wave is what determines the time-step constraints. In plasmas of propulsion interest, the fluid velocity is $\mathcal{O}(10^4)$ m/s. For a quasineutral plasma with charge density of $\mathcal{O}(10^{21})/\mathrm{m}^3$ and thermodynamic pressures of $\mathcal{O}(10^{-1})$ Torr and magnetic pressure of $\mathcal{O}(10^1)$ Torr, the fast magnetosonic wave speed is typically of the same order of magnitude as the flow velocity. This indicates that an explicit time marching scheme is suitable. From the CFL criterion, the time step for such a problem would be $\mathcal{O}(10^{-8} - 10^{-9})$ s.

Physical dissipation brings in different characteristic time scales into the problem. They are:

Magnetic diffusion: $= \mu_o \Delta r^2/\eta \quad \sim 10^{-10}$ s
Heat conduction: $= n_e k_B \Delta r^2/\kappa_{th} \sim 10^{-10}$ s
Viscous diffusion: $= \rho \Delta r^2/\mu_{visc} \quad \sim 10^{-9}$ s .

If these were vastly different, that would call for an implicit treatment of time stepping. That is not the case here, and an explicit time-stepping scheme was chosen.

Depending upon the particular case being simulated, the difference between convective and dissipative time scales could be more severe. Then, evaluating the convective fluxes at the time scales of dissipative fluxes would be prohibitively expensive. In order to sidestep this difficulty, a sub-stepping scheme can be chosen. In this method, the convective fluxes are updated only after N dissipative time steps, such that $N\Delta t$ is still less than the convective time scale.

2.3 Boundary Conditions

The boundaries in the computation of MPD flows are of various types. This section will discuss the estimation of the convective and dissipative terms at each type of boundary.

2.3.1 Flow Properties

The computational domain is assumed to be large enough such that there are no normal gradients in any of the flow properties at the free stream boundaries.

At solid boundaries, convective flux of all conserved variables, given by eqn.(1), is zero. For estimating the thermal conduction, either the temperature of the wall, or the heat flux to the wall has to be specified. A judicious estimate can be made for this, possibly from experimental data.

At the axis of symmetry, there are no radial convective fluxes. Moreover, there are no radial gradients. Therefore, there is no thermal conduction across the centerline.

At the inlet, a specified mass flow rate of the propellant enters at a specified temperature at sonic conditions. In reality, the propellant is injected as neutral gas at room temperature, and it gets almost fully ionized within a few millimeters from the inlet[23]. However, it is believed[24] that this ionization process cannot be modeled by fluid theory. Therefore, in this model, the inlet temperature is chosen to be high enough such that the propellant is sufficiently ionized. Effectively, the backplate of the numerical

model is not the true backplate, but a region few millimeters downstream of it.

2.3.2 Field Properties

The computational domain is chosen to be large enough such that all the current is enclosed within the domain. Thus, from Ampère's law, the magnetic field at free stream boundaries is zero. Note that if the domain is too small to make this assumption unreasonable, it will cause spurious jumps in flow variables, most notably in pressure.

At all other boundaries, the magnetic field is computed purely from Faraday's law. Using Stokes' theorem it can be written as,

$$\int_A \frac{\partial \mathbf{B}}{\partial t} \cdot d\mathbf{A} = -\oint_C \mathbf{E} \cdot d\mathbf{l} \ . \tag{5}$$

In the cell-centered scheme used in this work, eqn.(5) implies that the evolution of the magnetic flux is specified by the contour integral of electric field around the cell. Therefore, the only information required is the electric field drop along the boundaries.

At the axis of symmetry, the inductive component of the electric field is zero because there is no flow across it. The resistive component can be related to the magnetic field from the point next to $r = 0$, through a simple Taylor series expansion,

$$E'_z|_{r=0} = \eta j_z|_{r=0} = \frac{4\ B_\theta|_{\Delta r/2}}{\Delta r} \ . \tag{6}$$

From classical electromagnetic theory[25], the jump in the magnetic field, $\mathbf{H}_2 - \mathbf{H}_1$, across an interface between two media has to satisfy the relation,

$$\hat{\mathbf{n}} \times (\mathbf{H}_2 - \mathbf{H}_1) = \mathbf{J}_s \ , \tag{7}$$

where $\mathbf{J}_s$ is the surface current per unit length. Due to the no mass flux condition, the potential drop at a wall is entirely resistive, and is given by,

$$\mathbf{E}_w = \eta_w \mathbf{j}_w \ . \tag{8}$$

At conducting boundaries, all the current entering the discharge flows at the surface, at least in the transient case. Therefore, even though resistivity, η_w, for most conductors is very small, the electric field can be significant due to the large current density, in the transient case. In a true steady state, after the magnetic field has diffused into the conductor, the surface potential drop decreases to zero.

At insulated boundaries, the magnetic field diffuses into the wall instantaneously. Therefore, the jump in the the magnetic field, and subsequently the surface current is zero.

At the backplate, which also serves as the inlet, the total voltage drop is set as the boundary condition. Emulating a true constant current circuit, this applied voltage is adjusted every time step to maintain the specified amount of current to flow in the channel.

3 Improved Physical Model

3.1 Thermal Non-Equilibrium

For the conditions of interest, there is sufficient evidence (for instance, refs. [26], [27]) that electron and ion temperatures are different. Then, the disparity can be accounted for by using separate species energy equations. The conservation relation for the total internal energy, $\mathcal{E}_{int}$, of the fluid can be written as,

$$\frac{\partial \mathcal{E}_{int}}{\partial t} + \nabla \cdot [\mathcal{E}_{int}\mathbf{u}] + p\nabla \cdot \mathbf{u} = \mathbf{j} \cdot \mathbf{E} + \nabla \cdot (k_{th} \nabla T) \ . \tag{9}$$

The internal energy of the fluid can be further split into those pertaining to electrons, $\mathcal{E}_e$, and ions, $\mathcal{E}_i$, as

$$\mathcal{E}_{int} = \mathcal{E}_i + \mathcal{E}_e \ . \tag{10}$$

The electrical power input to the plasma, $\mathbf{j} \cdot \mathbf{E}$, can be split into the part that is expended in Ohmic heating, ηj^2, and the part that is used for accelerating the plasma, $(\mathbf{j} \times \mathbf{B}) \cdot \mathbf{u}$.

The thermal conductivity in the total energy equation is the sum of the contributions from both electrons and ions,

$$k_{th} \nabla T = (k_e \nabla T_e) + (k_i \nabla T_i) \ , \qquad (11)$$

where k_e and k_i are the coefficients of thermal conduction for the electrons and ions, respectively. With these assumptions, the conservation relations for the internal energy of electrons can be written as,

$$\frac{\partial \mathcal{E}_e}{\partial t} + \nabla \cdot [\mathcal{E}_e \mathbf{u}] + p_e \nabla \cdot \mathbf{u} = \eta j^2 - \Delta \dot{\mathcal{E}}_{ie} + \nabla \cdot (k_e \nabla T_e) \ , \qquad (12)$$

and that of ions as,

$$\frac{\partial \mathcal{E}_i}{\partial t} + \nabla \cdot [\mathcal{E}_i \mathbf{u}] + p_i \nabla \cdot \mathbf{u} = \Delta \dot{\mathcal{E}}_{ie} + \nabla \cdot (k_{th,i} \nabla T_i) \ . \qquad (13)$$

In the above expressions, p_e and p_i are the pressures of the electron and heavy species respectively, and ηj^2 is the Ohmic heating term, and $\Delta \dot{\mathcal{E}}_{ie}$ is the energy exchange term to be discussed later.

Since experimental data suggest that the disparity between the two temperatures is less than an order of magnitude, only one of eqns.(12) and (13) is needed, and the internal energy of the other species can be obtained, without significant error, by subtraction from the total energy. Note that the energy expended in acceleration, $(\mathbf{j} \times \mathbf{B}) \cdot \mathbf{u}$, does not appear in equations (12) and (13) because they are relations for the *internal* energy only. The acceleration energy would appear if the kinetic energy were also included in the definition of energy density.

It can be shown[28] that the ratio of thermal conductivities of electrons and ions depends upon the sqaure root of ratio of the masses of ions and electrons,

$$\frac{k_e}{k_i} \simeq \sqrt{\frac{M_i}{m_e}} \gg 1 \ . \qquad (14)$$

Since the temperatures of electrons and ions are not very disparate, one could make the assumption that thermal conduction of the ions is negligible compared to that of the electrons. However, there may be some regions, such as stagnation points, where thermal conduction may be an important energy dissipation mechanism for the ions. Therefore it is advisable to retain this term.

In eqns.(12) and (13), the rate of exchange of energy per unit volume between the electrons and the ions, through collisions, can be estimated as,

$$\Delta \dot{\mathcal{E}}_{ie} = \frac{3 \rho_e \nu_{ei}}{M_i} k_B \left(T_e - T_i \right) \ , \qquad (15)$$

where ρ_e is the electron mass density, and ν_{ei} is the average collision frequency between electrons and ions. Energy losses due to radiation are important in many types of plasmas. However, earlier work by Boyle[26], Villani[29], and Bruckner[27] suggests that the relative magnitude of this sink is not significant. Consequently, radiation losses will be ignored in the current model.

3.2 Equation of State

Real molecules possess internal energy in modes other than the translational. In these situations, the relationship between pressure, density and temperature is of the form

$$p = N k_B T \frac{\partial \ln Q}{\partial V} \ . \qquad (16)$$

Ignoring nuclear contributions, the total partition function, *Q* can be written as,

$$Q = Q_{rot} Q_{vib} Q_{tr} Q_{el} \ , \qquad (17)$$

where Q_{rot} is the contribution of rotational energy levels, Q_{vib} that of the vibrational energy levels, and Q_{el} that of the electronic energy levels.

Fortunately, most of the propellants of interest to plasma propulsion are monatomic in nature, and therefore, the rotational and vibrational contributions are absent. Thus the problem of finding the equation of state of a real gas reduces to the problem of estimating the electronic excitation partition function Q_{el}. These partition functions, for many elements of interest, can be found in references such as ref.[30]. Based on this work, Choueiri[31] derived expressions to obtain the temperature from pressure and density, for argon. As shown in Fig.(2), it is clear that at temperatures above 10^4K, the deviations from the ideal gas model are significant.

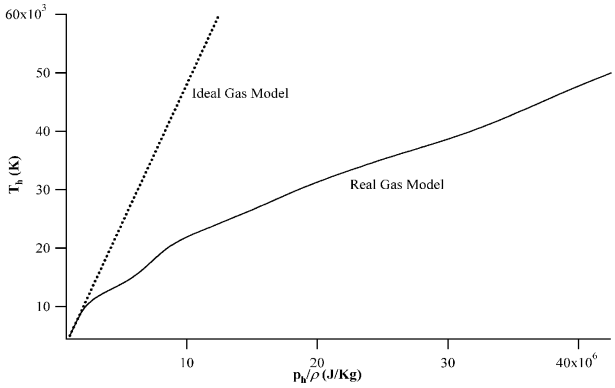

Figure 2: Deviation from ideal gas behavior for argon (calculated from data in ref.[30])

As energy is deposited into the internal modes, the ratio of specific heats also changes. Once again, this can be calculated from the data of partition functions. As seen in Fig.(3), the deviation from the ideal value of $5/3$ is severe at temperatures above 10^4K, which is consistent with Fig.(2).

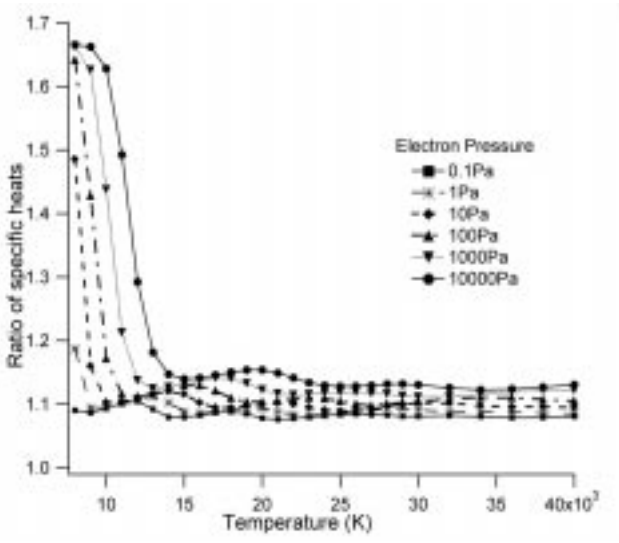

Figure 3: Variation of the ratio of specific heats for argon (calculated from data in ref.[30])

3.3 Anomalous Transport

It is known that the current can drive microinstabilities in the thruster plasma which may, through induced microturbulence, substantially increase dissipation and adversely impact the efficiency. The presence of microinstabilities in such accelerator plasmas has been established experimentally in the plasma of the MPDT at both low and high power levels[32], [33]. Choueiri[6] has developed a model to estimate the resulting anomalous transport and heating in terms of macroscopic parameters. Under this formulation, apart from the classical collision frequency of the particles, there exists additional momentum and energy transferring collisions between particles and waves. The resulting anomalous collision frequency is important whenever the ratio of electron drift velocity to ion thermal velocity, $u_{de}/v_{ti} \geq 1.5$. Above this threshold, the ratio of anomalous collision frequency to classical collision

frequency was found to depend on the classical electron Hall parameter, Ω_e, and the ratio of ion to electron temperatures, T_i/T_e. Polynomials giving these relations are in ref.[6] and are shown in Fig.(4).

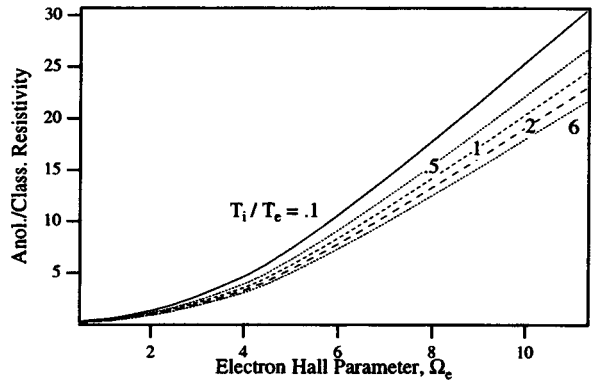

Figure 4: Ratio of anomalous to classical resistivity in argon plasmas (from ref.[6])

channel due to Hall effect. While the calculated values are in similar to the measured values withint the channel, the simulation does not predict the attachment pattern at electrode tips accurately. This can possibly be attributed to the unrealistic sharp corners of the electrodes in the simulation.

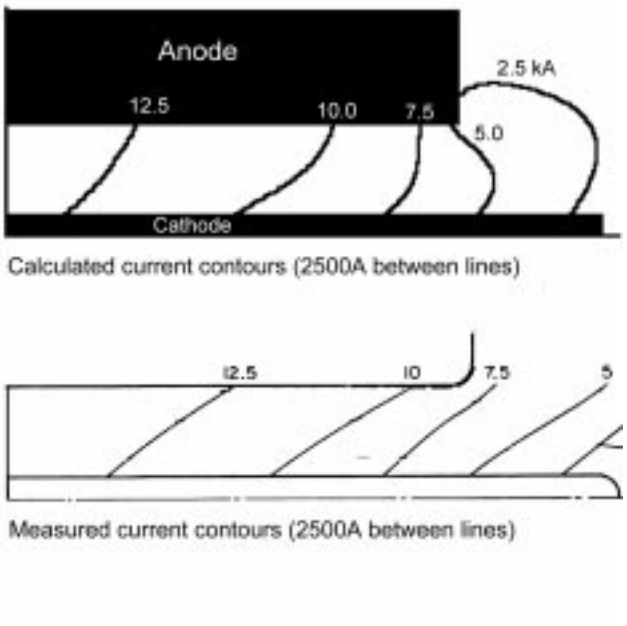

Figure 5: Contours of constant current (1000A between lines)

4 Results

4.1 Results from MPD Simulation

Due to the simple grid generation techniques used in this work, a constant area channel is a more amenable choice for study. The thruster chosen for simulation was a design used by Villani[29]. There exists sufficient data on the current and potential contours at various values of $J^2/\dot{m}$ for this geometry. The results shown are for argon mass flow rate of 6.0g/s and 15.0kA of discharge current, since these are common operating conditions for many MPDTs, for which experimental data exist.

The calculated and measured contours of enclosed current are shown in Fig.(5). They indicate the blowing of the current lines at the exit, due to convection, and also the canting of the current lines inside the

The current distribution on the surface of the cathode, shown in Fig.(6), shows peaks at the inlet (z=0), the anode length (z=0.20) and the cathode tip (z=0.264). This result is qualitatively in accordance with experimental observations.

The calculated contours of density are shown in Fig.(8). Within the channel, the axial component of the current produces a radial pumping force that pushes the plasma towards the cathode.

The calculated contours of axial velocity are shown in Fig.(7). The profile at the exit shows axial

velocities in the range of about 8.0 km/s to 14.0 km/s. This is in general agreement with range of measured values for this operating condition.

The profiles of heavy species temperature, shown in Fig.(8), indicate that it varies from about 1eV to about 3.5eV. These values are roughly in the range of experimental measurements in refs.[26], [27]. The stagnation point at the cathode tip is the region of highest temperature in the simulation.

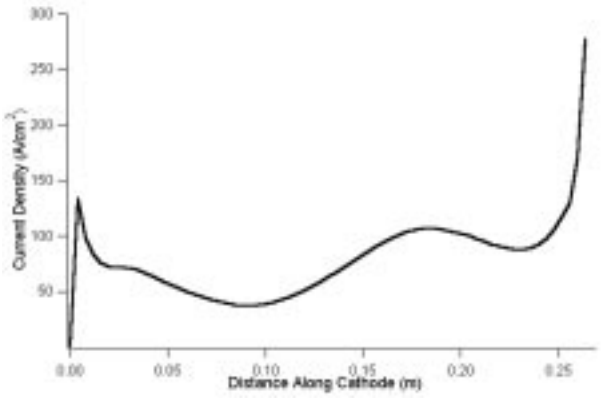

Figure 6: Current density distribution on cathode surface

4.2 Effect of Physical Models

To estimate the importance of the real equation of state model, described in §3.2, this part of the model was turned off and the code was run for the same operating conditions as in §4.1. The difference was very significant, not only in the values, but in the convergence itself. Without the real equation of state, the solution did not reach a steady state, as the heavy species temperature increased monotonically with time. An intermediate solution is shown in Fig.(8), and it can be seen that temperature exceeds 6.5eV. The explanation for the high temperature is simply, without energy expenditure into internal modes, namely electronic excitation and ionization, there are no sufficient energy sinks in the model.

Moreover, the density contours obtained with the ideal equation of state, shown in Fig.(8), are drastically different from the more realistic contours obtained with the real equation of state.

The effects of anomalous transport were not pronounced at these conditions, due to the correspondingly low values of the electron Hall parameter and u_{de}/v_{ti}. It is, however, interesting to note that anomalous transport effects appeared to be more important when the ideal equation of state was used instead of the real equation of state.

5 Concluding Remarks

The development and validation of a new solver to accurately compute plasma flows of interest to propulsion has been documented in earlier works by the authors (refs.[14] and [15]). In this paper, the utility of this solver to simulate plasma flows in magnetoplasmadynamic thrusters has been demonstrated. The calculated contours of velocity, density, enclosed current and temperature are in general agreement with measured values.

The robustness of this solver is evident from its ability to handle changes in the physical model, without requiring changes to the underlying scheme. In this paper, the effects of the real equation of state and anomalous transport models were included.

The effect of anomalous transport was found to have no major effect on the solution at this conditions. This can be explained to the lack of occurence of high electron Hall parameters for this geometry at this operating condition.

Though other researchers (ref.[13]) have found the ideal equation of state suitable to simulate MPDTs at lower current levels, for the chosen operating condition, $J = 15.0$kA, and $\dot{m} = 6.0$g/s, the real equation

of state was crucial to obtaining a realistic and stable solution.

References

[1] E. Y. Choueiri. *Advanced Problems in Plasma Propulsion*. Princeton U. Lecture Notes, 1998.

[2] K. Toki I. Kimura and M. Tanaka. Current distribution on the electrodes of MPD arcjets. *AIAA J.*, 20(7):889, 1982.

[3] T.Ao and T. Fujiwara. Numerical and experimental study of an MPD thruster. *IEPC-84-08*, 1984.

[4] T. Miyasaka and T. Fujiwara. Numerical prediction of onset phenomenon in a 2-dimensional axisymmetric MPD thruster. *AIAA-99-2432*, 1999.

[5] G. Caldo. Numerical simulation of MPD thruster flows with anomalous transport. Master's thesis, Princeton University, 1994.

[6] E.Y. Choueiri. Anomalous resistivity and heating in current-driven plasma thrusters. *Phys. Plasmas*, 6(5):2290, 1999.

[7] M. LaPointe. Numerical simulation of geometric scale effects in cylindrical self-field MPD thrusters. *NASA-CR-189224*, 1992.

[8] J.M.G. Chanty and M. Martinez-Sanchez. Two-dimensional numerical simulation of MPD flows. *AIAA-87-1090*, 1987.

[9] E. H. Niewood. *An Explanation for Anode Voltage Drops in an MPD*. PhD thesis, MIT, 1993.

[10] P.J. Turchi, P.G. Mikellides, K.W. Hohman, R.J. Leiweke, I.G. Mikellides, C.S. Schmahl, N.F. Roderick, and R.E. Peterkin Jr. Progress in modeling plasma thrusters and related plasma flows. *IEPC-95-159*, 1995.

[11] D.C. Lilekis and R.E. Peterkin Jr. Effects of azimuthal injection asymmetry of MPD thruster performance using the MACH3 code. *IEPC-95-2677*, 1995.

[12] H.J. Kaeppeler C. Boie, M. Auweter-Kurtz and P.C. Sleziona. Application of adaptive numerical schemes for MPD thruster simulation. *IEPC-97-115*, 1997.

[13] J. Heiermann, M. Auweter-Kurtz, J. J. Kaeppeler, A. Eberle, U. Iben, and P. C. Sleziona. Recent improvements of numerical methods for the simulation of MPD thruster flow on adaptive meshes. *IEPC-99-169*, 1999.

[14] K. Sankaran and E.Y. Choueiri. An accurate characteristics-splitting scheme for numerical solution of MHD equations. *IEPC-99-208*, 1999.

[15] K. Sankaran, L. Martinelli, and E.Y. Choueiri. A flux-limited numerical method for the MHD equations to simulate propulsive plasma flows. *AIAA-2000-2350*, 2000.

[16] R.G. Jahn. *Physics of Electric Propulsion*. McGraw-Hill, 1968.

[17] U. Shumlak, O. Jones, and S.D. Eberhardt. An implicit scheme for nonideal magnetohydrodynamics. *J. Comp. Phys*, 130:231, 1997.

[18] S.K. Godunov. Finite difference method for numerical computation of discontinous solution of the equations of fluid dynamics. *Matematicheskii Sbornik*, 47:15–21, 1959.

[19] S.K. Godunov. Symmetric form of the equations of magnetohydrodynamics. *Numerical Methods for Mechanics of Continuum Medium*, 1972.

[20] P. Roe. Approximate Riemann solvers, parameter vectors, and difference schemes. *J. Comp. Phys*, 43:357, 1981.

[21] P. Roe. Characteristics-based schemes for the Euler equations. *Annual Review of Fluid Mechanics*, 18:337, 1986.

[22] A. Jameson. Analysis and design of numerical schemes for gas dynamics, 1: Artificial diffusion, upwind biasing, limiters and their effect on accuracy and multigrid convergence. *Comp.Fluid.Dyn*, 1995.

[23] T. M. Randolph. Measurement if Ionization Levels in the Interelectrode Region of an MPD Thruster. Master's thesis, Princeton University, 1994.

[24] E.Y. Choueiri and H. Okuda. Anomalous ionization in MPD thrusters. *IEPC-93-067*, 1993.

[25] J.D. Jackson. *Classical Electrodynamics*. Wiley, 1975.

[26] M. J. Boyle. *Acceleration Processes in the Quasi-Steady Magnetoplasmadynamic Discharge*. PhD thesis, Princeton U., 1974.

[27] A. P. Bruckner. *Spectroscopic Studies of the Exhaust Plume of a Quasi-Steady MPD Accelerator*. PhD thesis, Princeton U., 1972.

[28] M. Mitchner and C.H. Kruger. *Partially Ionized Gases*. Willy-Interscience, 1973.

[29] D. D. Villani. *Energy Loss Mechanisms in a Magnetoplasmadynamic Arcjet*. PhD thesis, Princeton U., 1982.

[30] W. M. Sparks and D. Fischel. *Partition Functions and Equations of State in Plasmas*. NASA SP-3066, 1971.

[31] E. Y. Choueiri. A Scaling Strategy for the Preliminary Design of MPD Thrusters. Master's thesis, Syracuse University, 1983.

[32] E.Y. Choueiri, A. J. Kelly, and R.G. Jahn. Current-driven plasma acceleration versus current-driven energy dissipation: Part ii: Electromagnetic wave stability theory and experiments. *IEPC-91-100*, 1991.

[33] D.L. Tilley, E.Y. Choueiri, A. J. Kelly, and R.G. Jahn. Microinstabilities in a 10-kilowatt self-field magnetoplasmadynamic thruster. *J.Prop.Power*, 12(2):381, 1996.

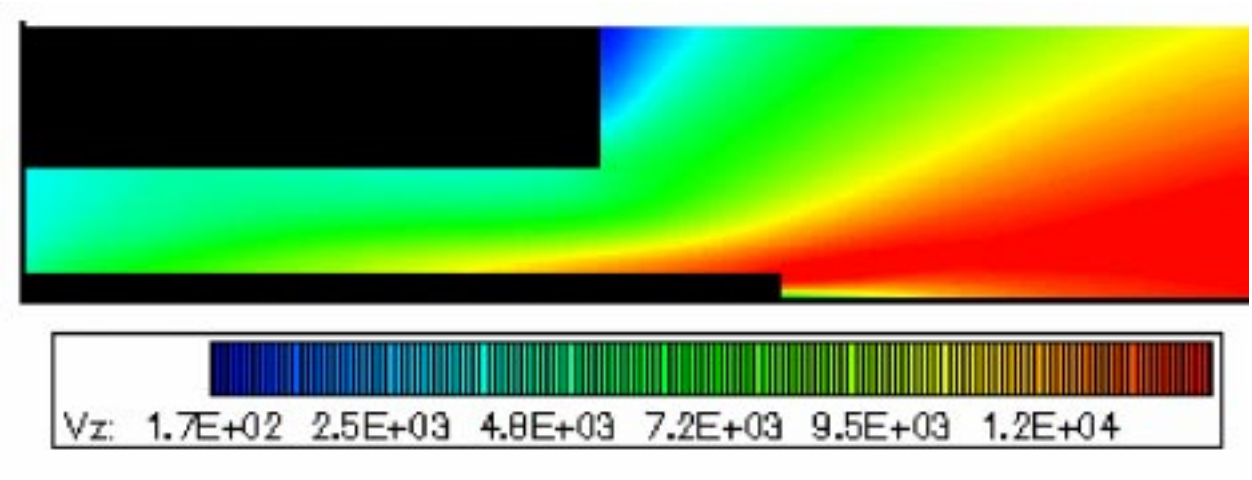

Figure 7: Axial velocity contours for 6.0g/s of argon and J=15.0kA

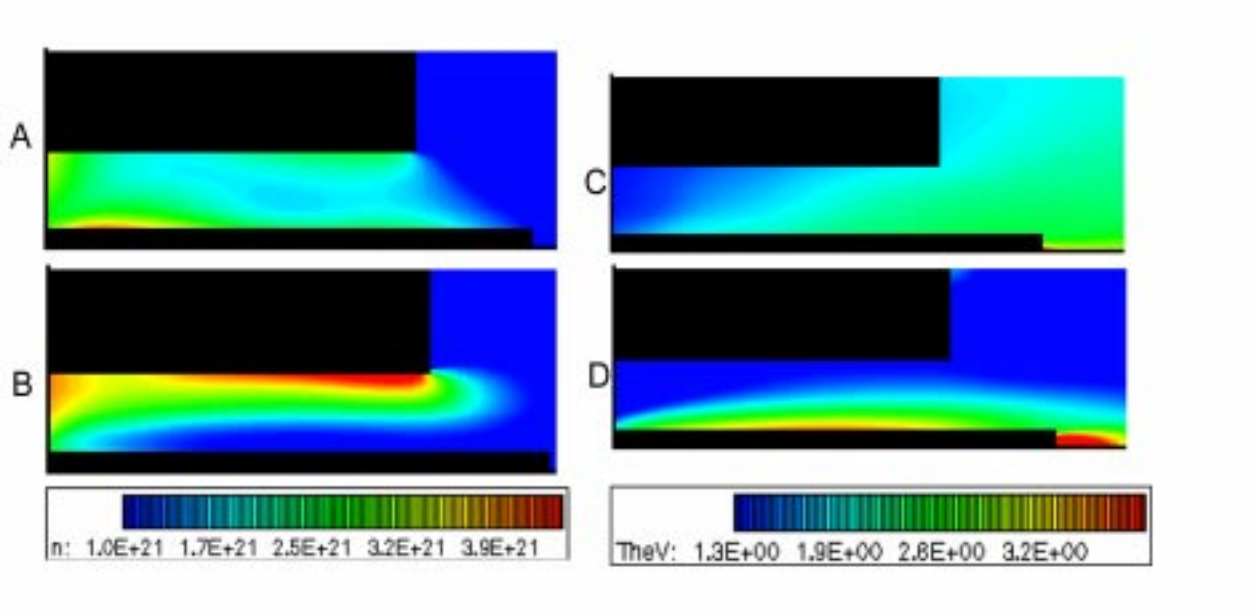

Figure 8: (a) Density profile with real equation of state; (b) Density profile with ideal equation of state; (c) Ion temperature with real equation of state; (d) Ion temperature with ideal equation of state